Supplement of Atmos. Chem. Phys., 22, 13341–13353, 2022
https://doi.org/10.5194/acp-22-13341-2022-supplement

Supplement of

Circulation-regulated impacts of aerosol pollution on urban heat island in Beijing

Fan Wang et al.

Correspondence to: Meng Gao (mmgao2@hkbu.edu.hk)

Table S1. Basic information of automatic weather stations in Beijing.

Station ID	Station Name	Longitude (°E)	Latitude (°N)
54399	Haidian	116.2906	39.9869
54406	Yanqing	115.9689	40.4494
54419	Huairou	116.6272	40.3575
54421	Shangdianzi	117.1117	40.6589
54424	Pinggu	117.1178	40.1694
54511	Guanxiangtai	116.4694	39.8061
54597	Xiayunling	115.7403	39.7289

Table S2. Basic information of CNEMC stations in Beijing.

Station ID	Station Name	Longitude (°E)	Latitude (°N)
1001A	Wanshouxigong	116.366	39.8673
1002A	Dingling	116.17	40.2865
1003A	Dongsi	116.434	39.9522
1004A	Tiantan	116.434	39.8745
1005A	Nongzhanguan	116.473	39.9716
1006A	Guanyuan	116.361	39.9425
1007A	Wanliu	116.315	39.9934
1008A	Shunyixincheng	116.72	40.1438
1009A	Huairou	116.644	40.3937
1010A	Changping	116.23	40.1952
1011A	Aotizhongxin	116.407	40.0031
1012A	Gucheng	116.225	39.9279

Table S3. Distribution of daily mean urban and rural $PM_{2.5}$ concentrations (unit: μg m^{-3}) under clean and polluted conditions ($PM_{2.5\_average}$ represents average $PM_{2.5}$ concentrations of all stations; $PM_{2.5\_urban}$ represents average $PM_{2.5}$ concentrations of all urban stations and $PM_{2.5\_rural}$ represents average $PM_{2.5}$ concentrations of all rural stations).

	$PM_{2.5\_average} \geq 75$ (369 days)	$PM_{2.5\_average} < 75$ (1373 days)
$PM_{2.5\_urban} \geq 75$	366 (99.19%)	18 (1.31%)
$PM_{2.5\_urban} < 75$	3 (0.81%)	1355 (98.69%)
$PM_{2.5\_rural} \geq 75$	306 (82.93%)	12 (0.87%)
$PM_{2.5\_rural} < 75$	64* (17.07%)	1361 (99.13%)

*: These 64 days consist of 4 days with $PM_{2.5\_rural} < 50$, 8 days with $50 \leq PM_{2.5\_rural} < 60$ and 52 days with $60 \leq PM_{2.5\_rural} < 75$.

Table S4. Average correlation coefficient (R), root mean squared error (RMSE) and mean error (ME) between observations and simulated 2m air temperature (T_{2m}, unit: °C), 10m wind speed (WS_{10m}, unit: m s^{-1}) and $PM_{2.5}$ concentration (unit: μg m^{-3}) in Case_2018.

	R	RMSE	ME
T_{2m}	0.98	1.84	1.35
WS_{10m}	0.57	1.98	1.52
$PM_{2.5}$	0.71	26.36	17.60

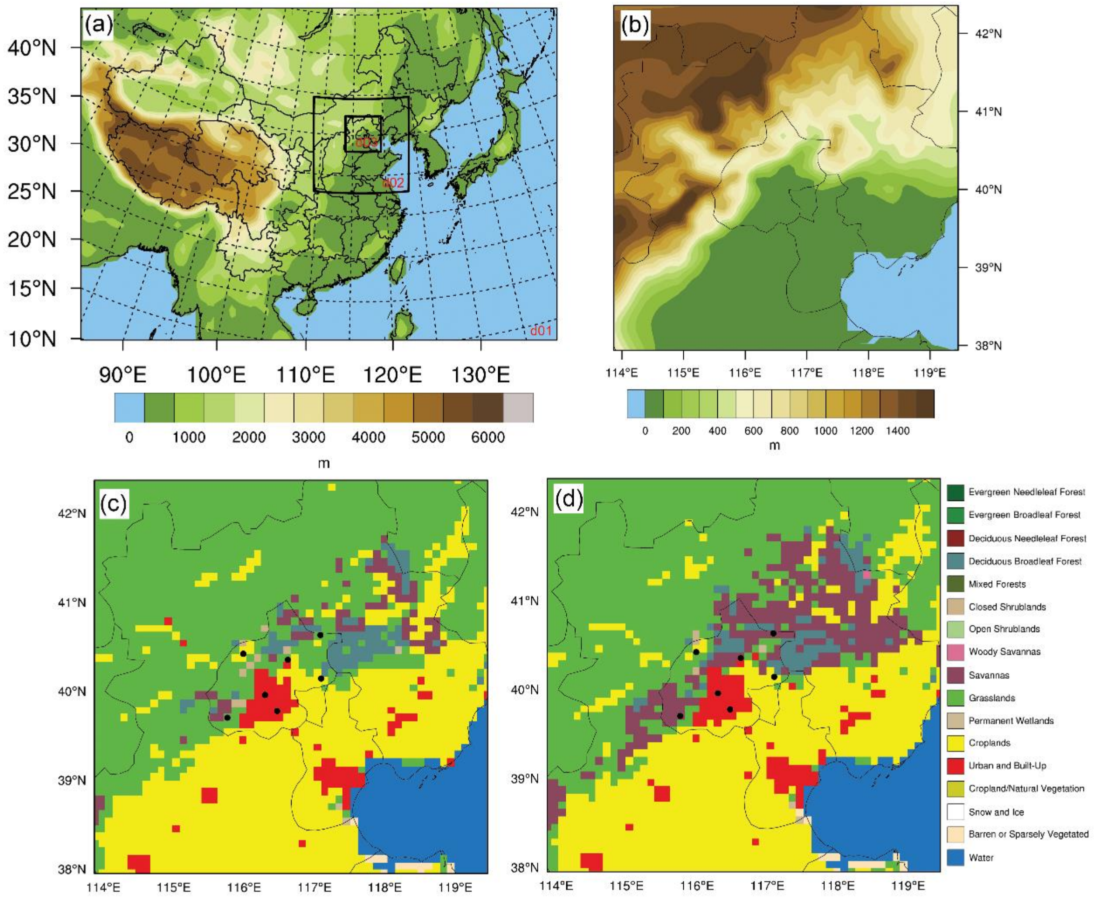

Figure S1. WRF-Chem domain configuration with terrain height (a), terrain height of the innermost domain (b), land use categories of the innermost domain of Case_2010 (c) and Case_2018 (d) (Black dots in b represent locations of automatic weather stations).

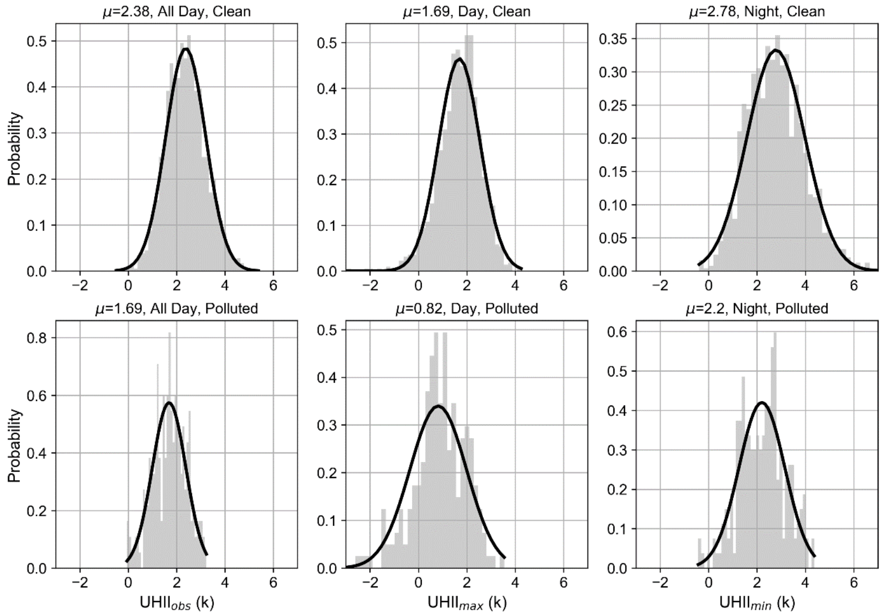

Figure S2. Probability distribution of $UHII_{obs}$ (a, d), $UHII_{max}$ (b, e) and $UHII_{min}$ (c, f) under different pollution conditions. Clean means $PM_{2.5}$ concentrations of all stations were < 75 μg m^{-3}, while polluted means $PM_{2.5}$ concentrations of all stations were ≥ 75 μg m^{-3}. The bold curve in each subgraph is normal distribution curve, and μ denotes the average value.

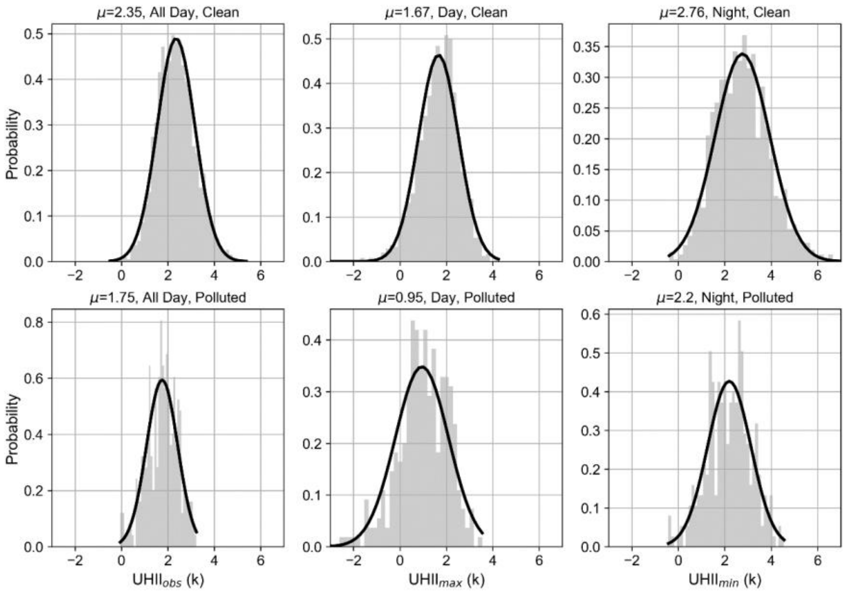

Figure S3. Probability distribution of $UHII_{obs}$ (a, d), $UHII_{max}$ (b, e) and $UHII_{min}$ (c, f) under different pollution conditions. Clean means both average $PM_{2.5}$ concentrations of all urban stations and those of rural stations were < 75 μg m^{-3}, while polluted means both average $PM_{2.5}$ concentrations of all urban stations and those of rural stations were ≥ 75 μg m^{-3}. The bold curve in each subgraph is normal distribution curve, and μ denotes the average value.

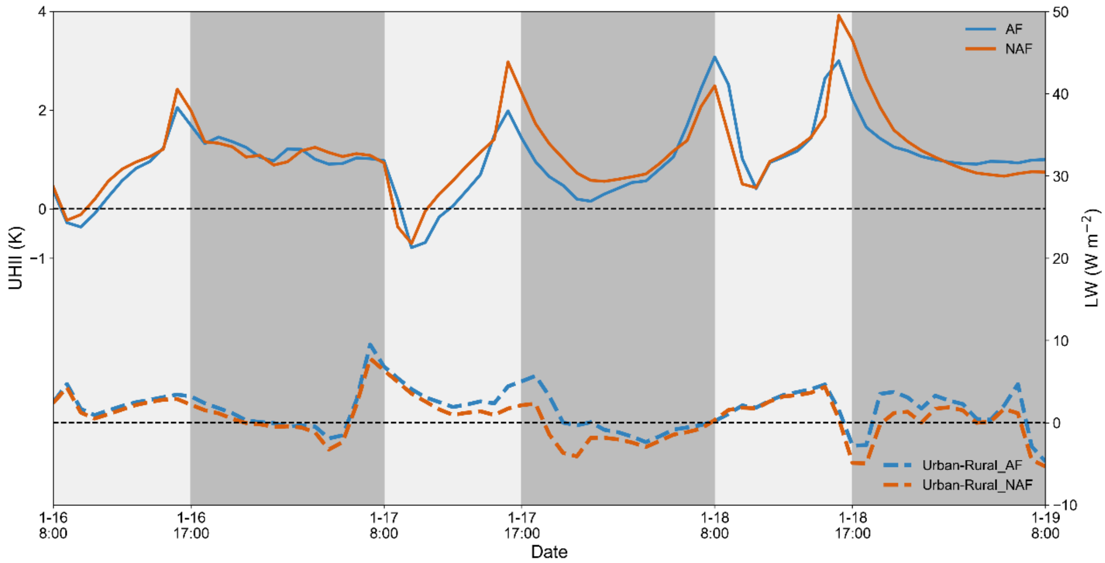

Figure S4. Variation of simulated UHII and downward longwave radiation at ground surface in Case_2010.

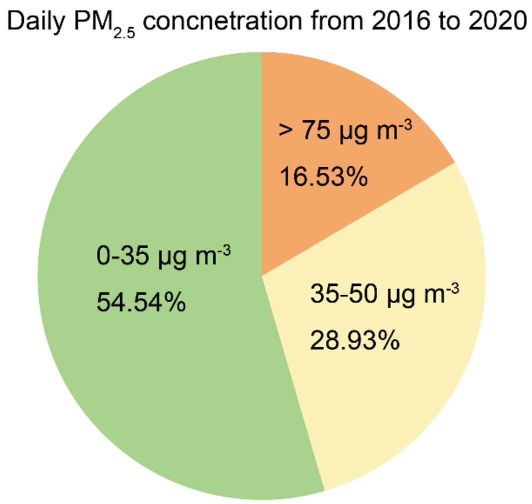

Figure S5. Distribution of daily average $PM_{2.5}$ concentration in different concentration intervals from 2016-2020 in 1002A and 1009A which located in north of Beijing.

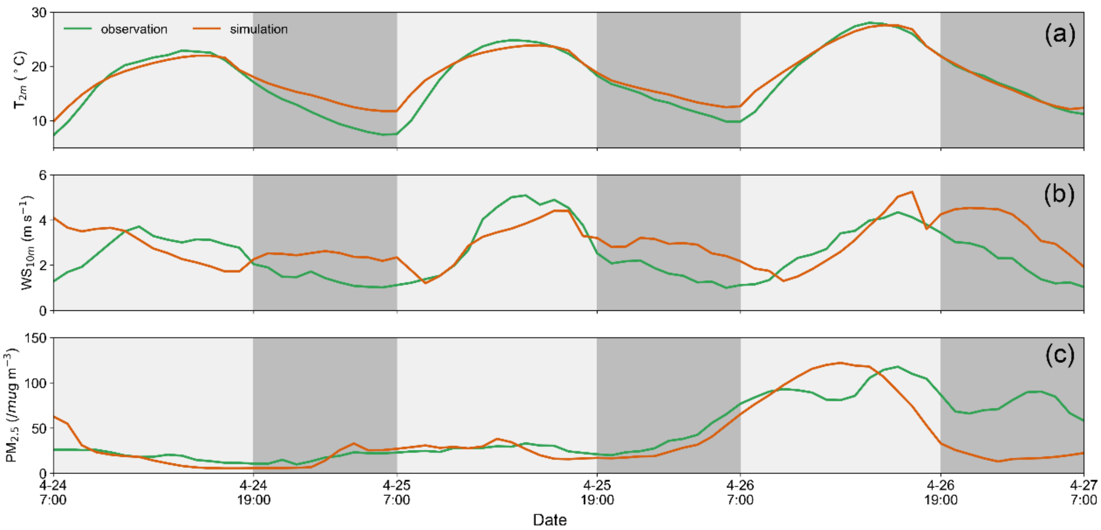

Figure S6. Simulated and observed 2m air temperature (a), 10m wind speed (b) and near-ground $PM_{2.5}$ concentration (c) in Case_2018. Observations are obtained from the stations listed in Table S1 and Table S2.

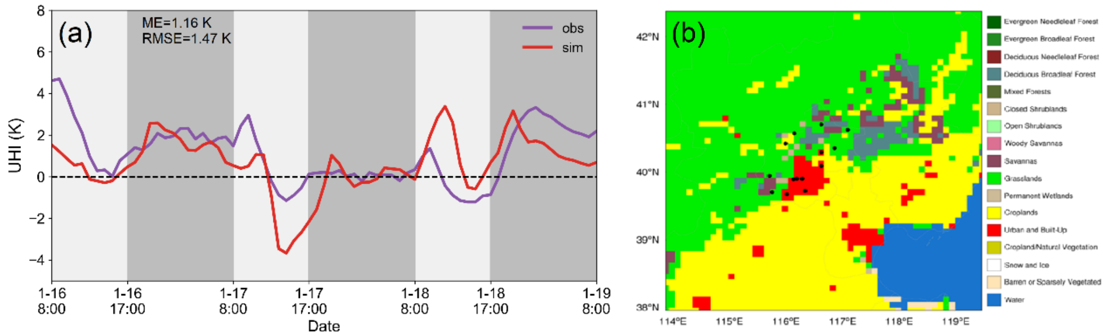

Figure S7. Observed and simulated UHII by AF in Case_2010 in Beijing (a) and the locations of the used sites (b). Simulated UHII here is site-based.

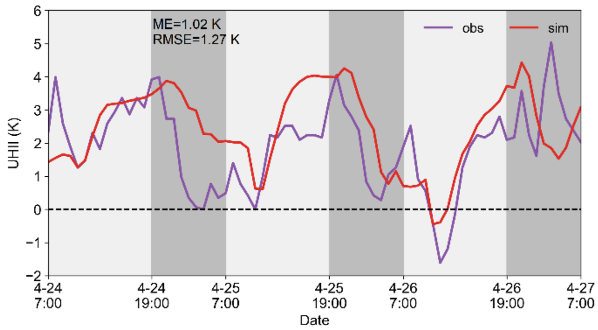

Figure S8. Observed and simulated UHII by AF in Case_2018 in Beijing. Observations are obtained from the stations listed in Table S1. Simulated UHII here is site-based.

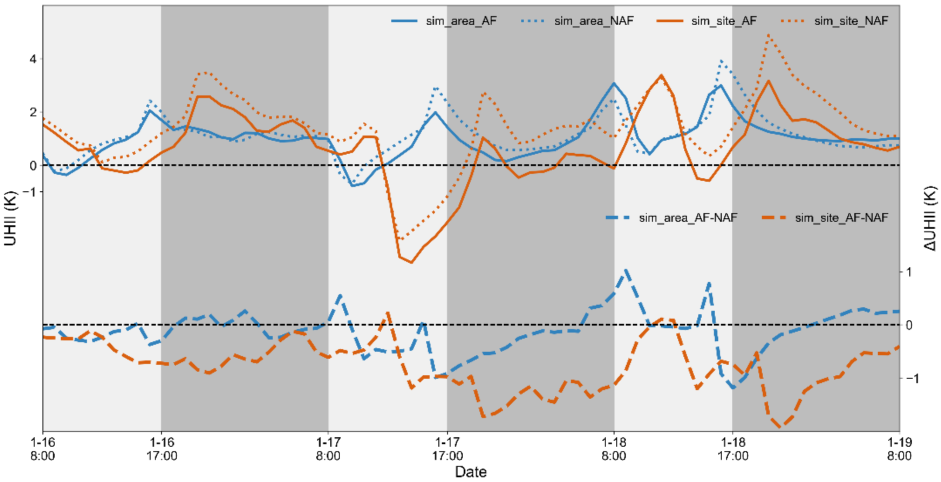

Figure S9. Variations of site-based and area-based UHII and difference between AF and NAF in Case_2010.

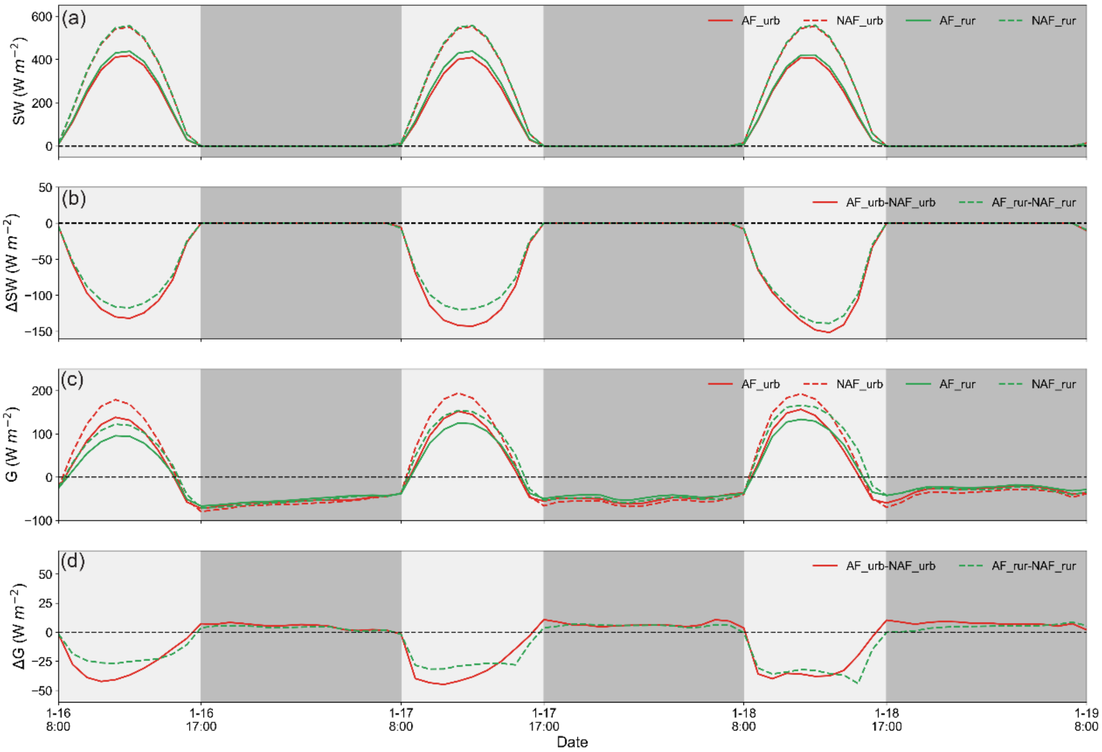

Figure S10. Variations of (a) downward shortwave radiation, (b) difference of downward shortwave radiation between AF and NAF, (c) heat storage and (d) difference in heat storage between AF and NAF in urban and rural areas in Case_2010.

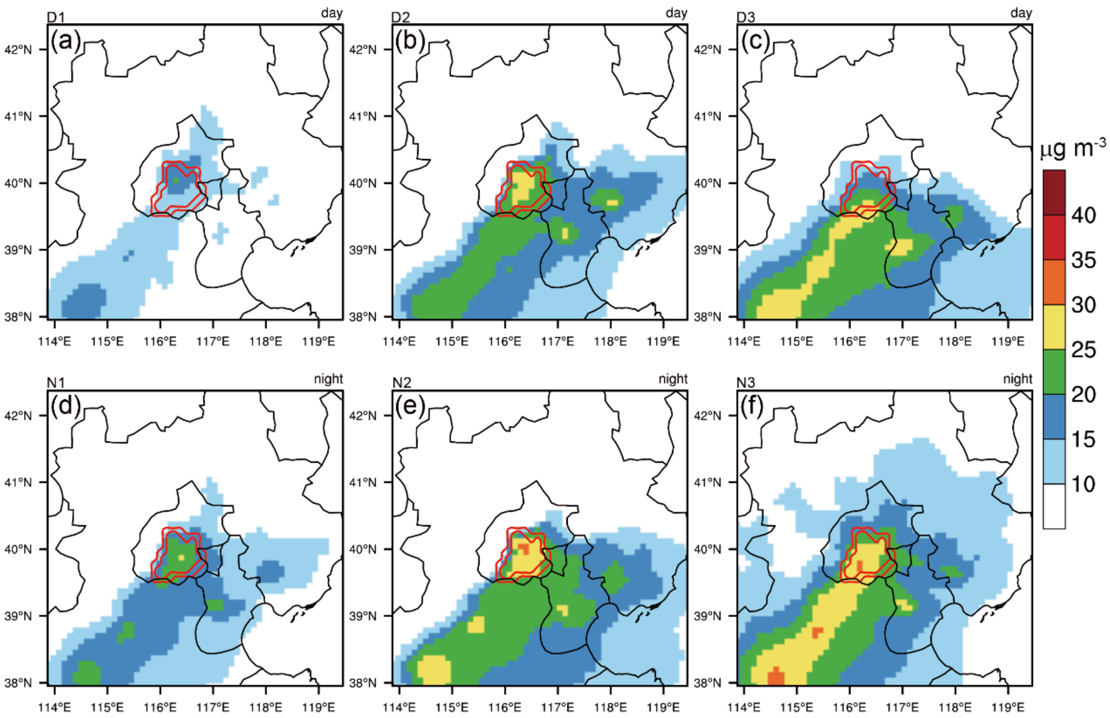

Figure S11. Simulated black carbon concentration on (a) D1, (b) D2, (c) D3, (d) N1, (e) N2 and (f) N3 in Case_2010. The areas within the inner red line are urban areas. The areas between the two red lines are rural areas having the same size as the urban areas.

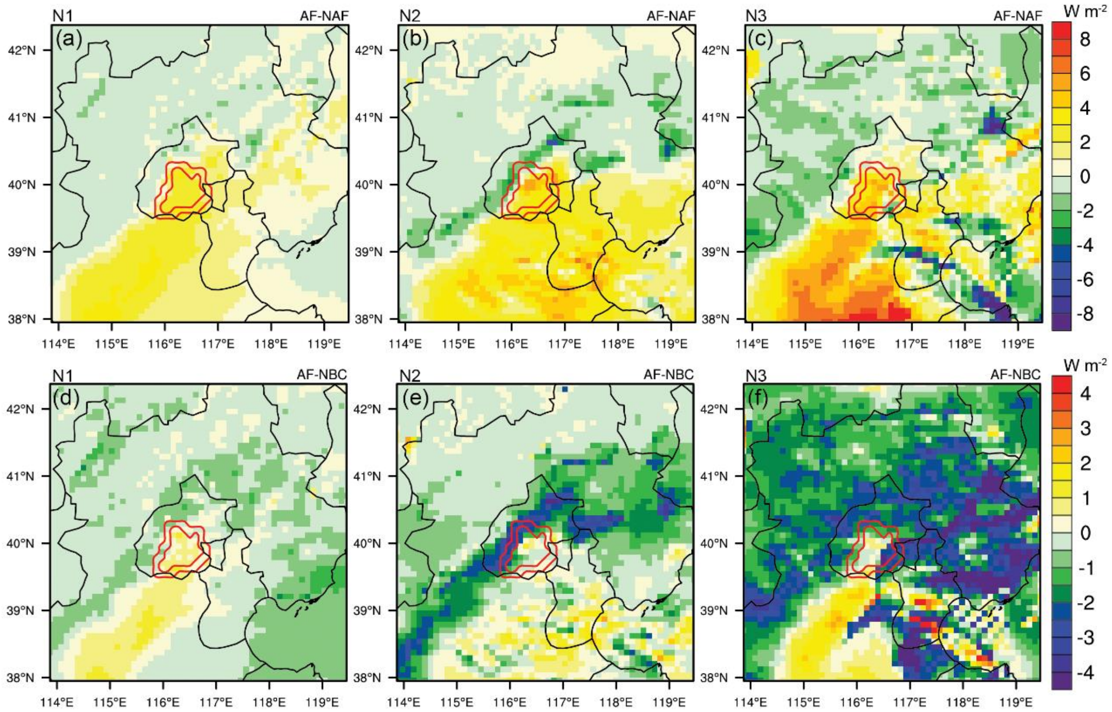

Figure S12. Simulated difference in downward longwave radiation between AF and NAF (first row), AF and NBC (second row) at nighttime in Case_2010. The areas within the inner red line are urban areas. The areas between the two red lines are rural areas having the same size as the urban areas.

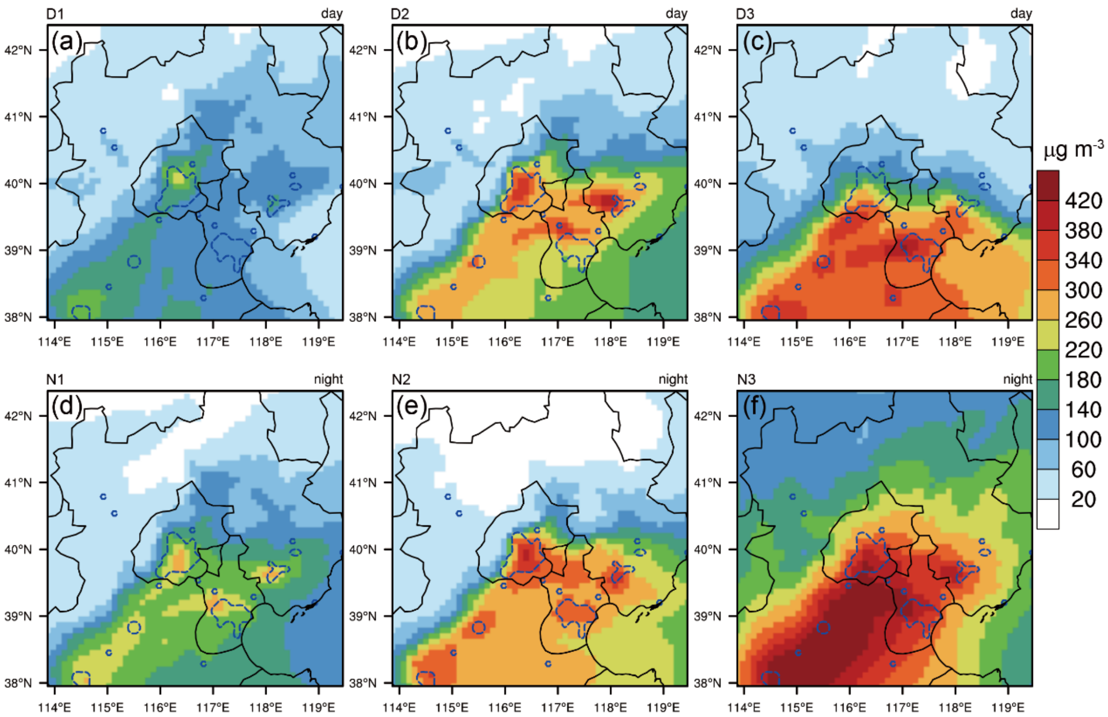

Figure S13. Simulated $PM_{2.5}$ concentration on (a) D1, (b) D2, (c) D3, (d) N1, (e) N2 and (f) N3 in Case_2010.

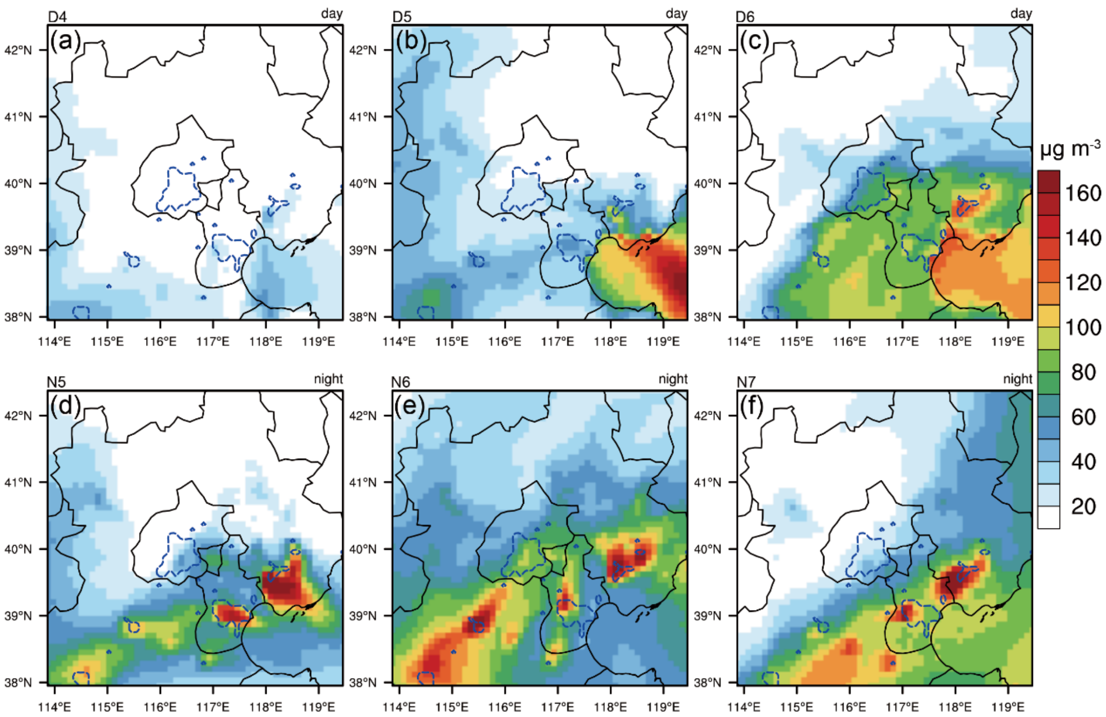

Figure S14. Same as Figure S11 but for Case_2018.

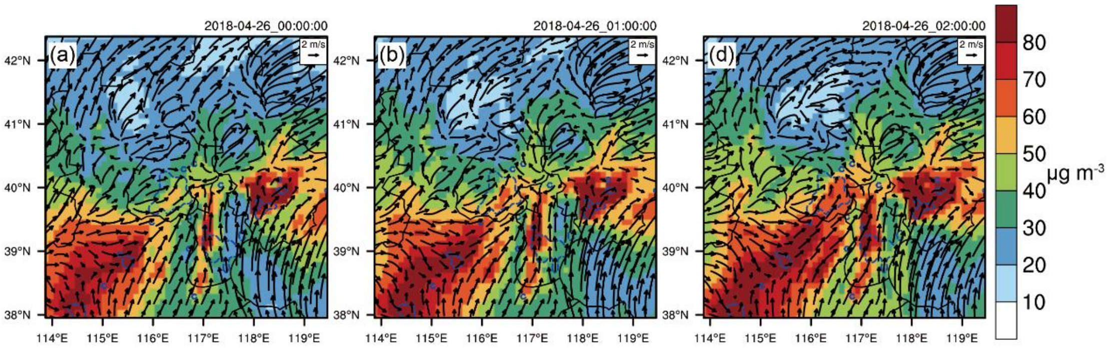

Figure S15. Simulated $PM_{2.5}$ concentration and 10m wind field at 00:00 (a), 01:00 (b) and 02:00 (c) on N5 in Case_2018.